Psychoacoustic Evaluation of an Array of Distributed Propellers Under Synchrophasing Operation

do Nascimento Monteiro, F.; Merino Martinez, R.; Lima Pereira, L.T.

DOI
10.2514/6.2024-3321

Publication date
2024

Document Version
Final published version

Published in
30th AIAA/CEAS Aeroacoustics Conference (2024)

Aeroacoustics Conferences
June 4-7, 2024, Rome, Italy
30th AIAA/CEAS Aeroacoustics Conference (2024)

10.2514/6.2024-3321

Psychoacoustic Evaluation of an Array of Distributed Propellers Under Synchrophasing Operation

Fernanda do N. Monteiro*, Roberto Merino-Martínez†, and Lourenço T. Lima Pereira‡
Delft University of Technology, Delft 2629HS, The Netherlands

This preliminary study evaluates the expected psychoacoustics annoyance of an array of distributed propellers operating at different synchrophasing angles between the propeller blades. The study, conducted in a hybrid test section wind tunnel, focused on a three-propeller array in a tractor configuration. The noise emissions were measured using a phased microphone array. Both conventional noise metrics and state-of-the-art psychoacoustic metrics were calculated, enabling a thorough analysis of the noise characteristics produced by these configurations and their expected noise perception. The study found that the relative blade-phase angle significantly influences the levels of the conventional noise metrics and psychoacoustic metrics. These results highlight the potential of controlling relative blade-phase angles to reduce noise annoyance. They also emphasize the importance of conducting psychoacoustic analysis in design configurations like the one examined here.

Nomenclature

BPF	=	blade-passing frequency, Hz
d	=	separation distance between propellers, m
D	=	diameter, m
f	=	frequency, Hz
FS	=	fluctuation strength, vacil
J	=	advance ratio
K	=	tonality, t.u.
L_p	=	sound pressure level, dB
$L_\mathrm{p,A}$	=	A-weighted sound pressure level, dBA
n	=	rotational speed, Hz
N	=	loudness, sone
OASPL	=	overall A-weighted sound pressure level, dBA
OSPL	=	overall sound pressure level, dB
PA	=	psychoacoustic annoyance, –
PNLT	=	tone-corrected perceived noise level, PNLTdB
r	=	radial coordinate, m
R	=	roughness, asper
R_p	=	propeller radius, m
S	=	sharpness, acum
SPL	=	sound pressure level, dB
U_∞	=	freestream velocity magnitude, m s^{-1}
X, Y, Z	=	Cartesian coordinates, m
α	=	angle of attack, °
β	=	blade pitch angle, °
$\Delta\phi$	=	relative blade-phase angle, °
θ	=	propagation angle, °

*PhD Candidate, Wind Energy Section, Fac. of Aerospace Eng., and AIAA Member, F.doNascimentoMonteiro@tudelft.nl.
†Assistant Professor, Aircraft Noise and Climate Effects Section, Fac. of Aerospace Eng., R.MerinoMartinez@tudelft.nl, AIAA Member.
‡Assistant Professor, Wind Energy Section, Fac. of Aerospace Eng., L.T.LimaPereira@tudelft.nl, AIAA Member.

Subscripts

max	=	maximum value
p	=	propeller quantity
w	=	wing quantity
5	=	5% percentile value
∞	=	freestream quantity

I. Introduction

The aviation industry offers significant economic and social advantages, promoting innovation and improving global connectivity. Nevertheless, growing public awareness of the environmental repercussions of aviation, including CO_2 emissions, harmful noise levels, local air pollution, and other non-CO_2 emissions contributing to climate change, has spotlighted the need for sustainable development of aviation technology. Consequently, international organizations have stipulated quantitative targets for reducing chemical pollutants and noise pollution for future aviation. For instance, Flightpath 2050 has established targets for aircraft in operation by the year 2050 to cut down CO_2 emissions by 75%, NO_x emissions by 90%, and to decrease the perceived noise levels by 65% compared to the levels from new aircraft in the year 2000 [1].

As the industry grows and the demand for sustainable aviation increases, Urban Air Mobility (UAM) is emerging. It aims to provide a safe and efficient system for passenger and cargo transport within urban areas [2]. Its goal is to reduce road congestion, improve mobility, shorten transport times, and decrease pollution [3]. UAM vehicles offer the potential for very low to zero emissions and lower noise levels than traditional aircraft, representing an exciting paradigm shift in aviation. However, there are challenges to implementing this technology, such as regulatory approval, certification, weather conditions, and urban infrastructure [3]. Social concerns about safety, privacy, and noise also need consideration [2, 4].

Distributed Electric Propulsion (DEP) systems are often proposed as a solution to current aviation objectives [5] and are a popular choice for new Urban Air Mobility (UAM) aircraft design. DEP technology combines aerodynamics and propulsive systems to enhance overall performance. Unlike traditional configurations, DEP systems can separate the propulsor from its energy source, providing more design flexibility. This means propulsors can be strategically placed across the airframe to enhance the vehicle's aerodynamics, structural design, control, and acoustic emissions [6–8]. Given the relatively consistent efficiency of electric motors across different sizes [6, 9], this concept allows designers to choose from a broader range of propulsor sizes, further expanding the aircraft's design possibilities.

Propellers are a common design choice in UAM aircraft and DEP configurations. When seen as a standalone component, they are known for their high efficiency at low to moderate flight Mach numbers. This efficiency is achieved by generating thrust through the moderate acceleration of a large mass of air. Usually, the larger the acceleration, the more energy is needed to convert into mechanical energy. Therefore, propellers consume less energy, making them more cost-effective. Propellers also have lower manufacturing and maintenance costs than other propulsion methods [10].

Despite their benefits, propellers produce substantial noise levels at high tip speeds [9]. However, in a configuration incorporating multiple propellers, the total thrust required by the aircraft is distributed amongst several elements. Consequently, each propeller needs to provide less thrust, which allows for a reduced size. This approach also decreases the Mach tip number, significantly reducing the noise each propeller produces. Furthermore, electric motors typically have a lower acoustic impact than gas turbines [7]. Thus, at first glance, such configurations could offer significant noise reduction. However, propellers lack the beneficial noise-shielding effect that the nacelle in turbofan engines provides [11], and thus, noise reduction measures, such as acoustic lining, cannot be applied [12]. Nonetheless, solutions exist to reduce and control DEP aircraft noise, such as synchrophasing.

Synchrophasing considers each propeller as a separate acoustic source and, by adjusting the relative blade-phase angle $\Delta\phi$ between them, generates destructive interference at the emitted blade passing frequency (BPF) at specific locations, consequently reducing the noise levels at target areas. Utilized initially to minimize cabin noise in conventional aircraft [13–15], the broader implications of synchrophasing for community noise reduction are gaining attention in DEP studies [16–18]. In recent work, Patterson et al. [18] proposed a method for generating flight trajectories for DEP aircraft with synchrophasing. The simulation required the vehicle to navigate an urban environment with both spatial and acoustic constraints. The aircraft adjusted the propeller phase angles to direct noise away from specific locations and, consequently, satisfy noise constraints in sensitive areas on the ground. The results showed promising noise reductions beneath the aircraft as the angle between propeller blades was varied.

Although these studies reveal the potential for active noise control in DEP configurations, they only consider acoustic

interference, assuming that the propeller operates in undisturbed flow. However, in the highly integrated systems inherent to DEP configurations, substantial interference between aircraft components is inevitable. In fact, a key advantage proposed for DEP systems is the strategic exploitation of synergistic interactions and integrations between the propulsion and airframe systems. This high level of integration suggests that the flow field of one component will significantly influence the flow field of others, leading to a complex interplay of aerodynamic effects.

Several studies have highlighted the significant role of aerodynamic interference on the acoustic emissions of distributed propeller systems. For instance, Zhou et al. [19] found that rotor-to-rotor interactions in small Unmanned Aerial Vehicles (UAVs) can cause a significant increase in thrust fluctuations and noise levels. Similarly, the experimental study performed by de Vries et al. [20] demonstrated that the aerodynamic interaction in an array of propellers changes the system's acoustic waveforms, making them differ from the superposition of isolated propellers. Also, their research indicated that noise directivity can be controlled by adjusting the relative phase angle between propellers. Further supporting these findings, a numerical investigation by Zarri et al. [21] confirmed that adjacent propellers can increase the unsteadiness of the blade loading and result in higher noise emissions. This effect is especially pronounced along the propeller rotation axis. In contrast, for an isolated propeller operating in a uniform inflow, the noise directivity reaches a minimum for listeners placed in the direction of the axis of rotation. These findings highlight the significant influence of aerodynamic interference on the acoustic emissions of distributed propeller systems, underlining the need for more research in this field.

While questions remain about understanding the impact of flow phenomena on DEP noise, another critical aspect is human perception of the noise emitted from these systems. For instance, UAM vehicles produce different noise profiles from traditional aircraft, with characteristics such as tonality that could potentially increase annoyance [22]. The close proximity of UAM aircraft routes to populated areas further complicates the matter. According to a 2021 report by the European Union Aviation Safety Agency (EASA) [4], safety was the primary concern for EU citizens regarding UAM, with noise coming in a close second. A noise perception survey revealed that the noise of a UAM vehicle is deemed more bothersome than familiar noises at the same maximum noise level. This result suggests that unfamiliar sounds or specific characteristics of the noise profile emitted by these aircraft may trigger more negative responses. Thus, comprehending noise perception related to unconventional aircraft is vital for successfully implementing UAM technology. This understanding will influence UAM design, legislation, and planning for infrastructure and routes.

Regarding DEP systems, the combined sound produced by multiple propellers can generate amplitude and phase modulations. Current research in this area is limited, and the human response to these sounds remains insufficiently investigated. Traditional noise certification metrics, such as the maximum A-weighted sound pressure level (LA_{max}), may not accurately reflect the annoyance potentially caused by these sounds [23]. This uncertainty highlights a significant gap and indicates a need for further psychoacoustic research to discern the differences and evaluate the applicability of metrics and predictive models. Rizzi et al. [23], in one of the few studies dedicated to the psychoacoustics of distributed propeller systems, developed an annoyance model using loudness, roughness, and tonality as predictors. Additionally, in their psychoacoustic test, it was found that the mean annoyance response varies significantly with the number of propellers and the inclusion of time-varying effects, but it does not differ significantly with the relative RPM between propellers.

While Rizzi et al.'s research was a first step, there are still many gaps related to DEP aeroacoustics and its impact on hearing perception. As stated above, there is a keen interest in understanding the impact of aerodynamic interference on the acoustic emissions of distributed propeller systems. This interest primarily stems from the need to mitigate noise level emissions by effectively employing synchrophasing to control the noise emitted by DEP systems. However, even with the ability to steer noise emissions away from target areas using synchrophasing, the question remains: Will the noise level reduction be perceptible to the human ear? Or could the altered noise characteristics resulting from synchrophasing increase annoyance levels?

This paper aims to address these questions by delving deeper into the psychoacoustic aspects of DEP systems. By doing so, it contributes to the development of more effective noise mitigation strategies for innovative aircraft designs. Therefore, the present study aims to use psychoacoustic metrics to evaluate the potential of controlling the relative propeller blade phase angle ($\Delta\phi$) for reducing the noise annoyance caused by DEP aircraft. To this end, an experimental wind-tunnel campaign was conducted featuring an array of three identical propellers mounted in a tractor configuration mounted on a hybrid-anechoic test section. The noise emissions of different configurations were measured using a phased microphone array and evaluated using conventional and psychoacoustic sound metrics.

The paper is structured as follows: Section II) details the wind-tunnel facility, experimental model, test conditions, and acoustic measurements were performed. This is followed by the methodology (section III), where the signal processing and sound quality metric used to derive the data are discussed. The findings are then presented and discussed

in section IV. The paper concludes with a summary of the main findings and a discussion of future research directions (section V).

II. Experimental Setup

This section provides a detailed overview of the experimental setup and procedures used in the research. It starts by explaining the modifications made to the wind tunnel to accommodate aeroacoustic studies, followed by the experimental model description, i.e. an array with three propellers arranged side-by-side in close proximity, positioned upstream of a wing. Further, the test conditions are described, including the specific setups of the propellers and the wing. It concludes by explaining the methods used for acoustic measurements and data acquisition properties.

A. Wind-tunnel facility, model description and test conditions

The experiments were conducted in the Low Turbulence Tunnel (LTT) at Delft University of Technology, a closed-circuit wind-tunnel facility. The wind-tunnel features a contraction ratio of 17.8, yielding freestream turbulence levels in the test section from 0.04% at a flow velocity of 20 m/s up to 0.1% at 75 m/s [24]. Its octagonal test section has dimensions of 1.80 m wide, 1.25 m high, and 2.60 m long.

The LTT was originally designed for aerodynamic testing. However, one of its test sections was modified to accommodate aeroacoustic studies (see Fig. 1a). As a result of these modifications, the ceiling and floor of the acoustic test section are lined with 30 mm melamine foam, and the side walls are comprised of 50 mm-thick wedged melamine foam covered with a Kevlar sheet to achieve a smoother surface. For performing acoustic measurements, one of the side panels is replaced with a tensioned Kevlar window, behind which a phased microphone array is positioned (Fig. 1b). This arrangement protects the microphones from the hydrodynamic pressure fluctuations from the turbulent boundary layer formed over the wind-tunnel walls while still allowing acoustic waves to pass through [25]. Ramps are placed upstream and downstream of the melamine panels to prevent the lining on the ceiling and floor from being affected by flow stagnation and separation. The works of Bento et al. [26, 27] provide further information on the acoustic properties of the adapted test section.

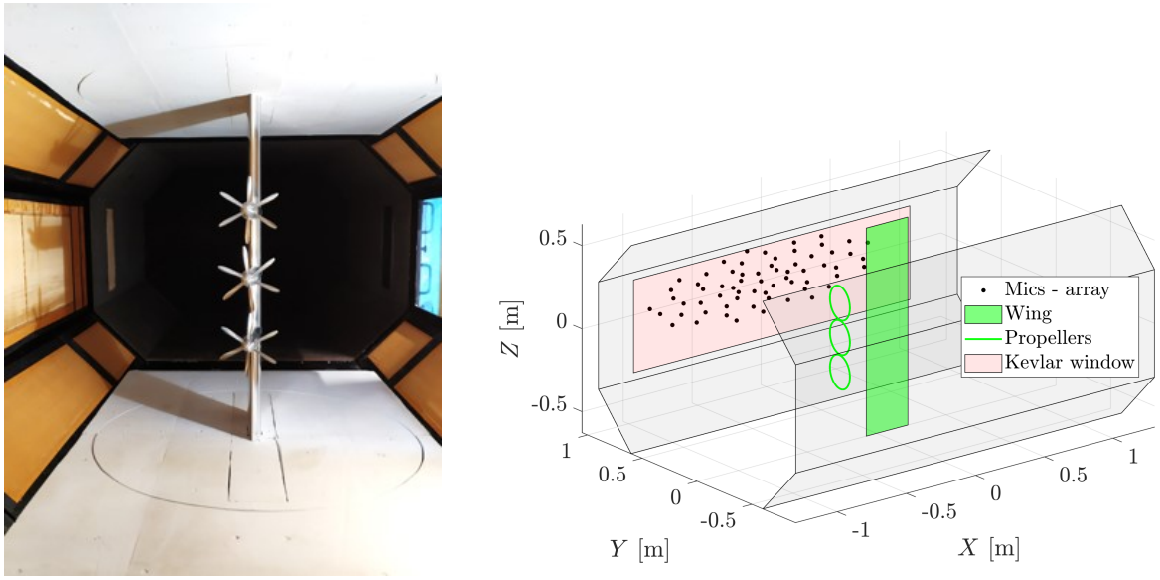

(a) **(b)**

Fig. 1 Experimental setup inside the acoustic test section (1a) and microphone positioning behind the Kevlar window (1b).

The experimental setup consists of three identical six-bladed steel propellers, known as XPROP-S. Each propeller has a radius of $R_p = 101.6$ mm and is arranged side by side, positioned about $0.85D_p$ away from the leading edge of a wing, and angled 5° downward relative to the wing chord. The wing, featuring an NLF-Mod22(B) airfoil [28], is untapered, unswept, and has a chord length of 0.3 m and a span of 1.25 m. The middle propeller and nacelle are located

on the wing's centerline. A tip clearance of $0.05R_p$ (4.8 mm) is maintained between adjacent propellers. The entire assembly is vertically placed within the wind-tunnel test section, as shown in Fig. 1a. The characteristics of the blade, distributed radially, are illustrated in Fig. 2a. Furthermore, Fig. 2b juxtaposes the performance of a propeller in an isolated case and when placed in the middle of a distributed propeller setup, as researched by de Vries et al. [20]. It should be noted that no wings were present in the study de Vries et al., and the clearance between the propellers was marginally closer, with a gap of 4 mm. This suggests that the propulsive-efficiency losses caused by interactions between rotors should be less in the current study [16].

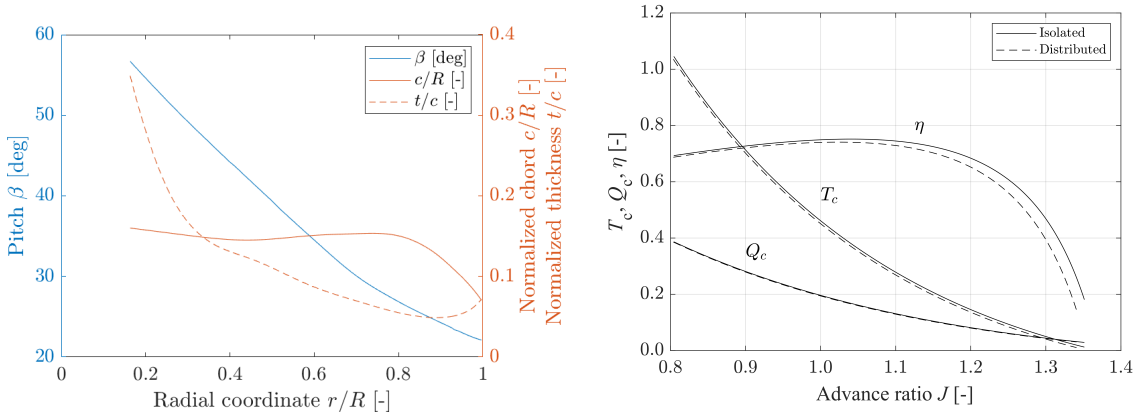

(a) **(b)**

Fig. 2 Characteristics of blade geometry (2a) and performance of the propeller in both isolated and distributed array configurations (2b). Figure 2b adapted from Ref. [20]

Each propeller is powered by a brushless DC electric motor housed within the aluminum nacelles. The motors are controlled by a dedicated PWM-controlled trapezoidal electronic speed controller (ESC) and powered by an external programmable 5 kW DC power supply. Motor constraints limited the propellers to a rotational speed of 184.55 Hz (≈11,000 RPM). At the freestream flow velocity of $U_\infty = 30$ m/s set for the experiment, this condition translates to an advance ratio $J = U_\infty/(nD_p)$ of 0.8. This corresponds to isolated-propeller thrust coefficients of approximately $T_c = 1.05$ (see Fig. 2b), a blade tip Mach number of 0.35, and Reynolds numbers at the tip of approximately 6.0×10^4.

A total of six different relative blade-phase angles $\Delta\phi$ (Fig. 3) were tested: 0°, 10°, 20°, 30°, 40°, and 50°, as well as a baseline case with random $\Delta\phi$ values. These random values were obtained by slightly increasing the speed of the two outer propellers relative to the middle one by a difference of 0.03 Hz. This difference allowed the angle $\Delta\phi$ to shift gradually during the acquisition time of each measurement point, covering about one full rotation (0° to 360°). The offset in rotational speed corresponded to a difference of advance ratio below 0.03%, which should have a negligible effect on propeller performance. Custom-made software controlled the rotational speed and the relative blade-phase angle among propellers, which resulted in a standard deviation of 0.01 Hz in rotational speed and below 0.16° in relative blade-phase angle. This deviation from the nominal rotation rate provided sufficient precision to analyze the effect of synchrophasing on the noise emissions of distributed propeller systems.

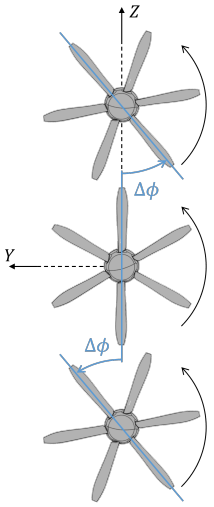

Fig. 3 Definition of relative blade-phase angle $\Delta\phi$.

Concerning the selection of the angle of attack for the wing, it is essential first to comprehend the impact of the wing on the upstream propellers. The wing's upwash can affect the propeller's performance by altering the flow direction upstream from the wing and, consequently, modifying the local angle of attack that propeller blades experience during a rotation. In this initial study, it was decided to mitigate this by choosing an angle of attack such that the upwash effect aligns the local flow direction with the upstream propellers' axis. For this experimental model, and at a freestream velocity of 30 m/s, this alignment occurs when the wing's angle of attack is approximately $\alpha_w = 2°$. While the propellers still encounter the blockage effect from the downstream wing, this test condition should reduce fluctuations in the blade's local angle of attack caused by the wing, allowing for a more efficient study of rotor-rotor interference impact.

To conclude this subsection, an overview of the test conditions considered in the experimental

campaign is gathered in Table 1.

Table 1 Overview of test conditions considered.

Parameter	Evaluated values
Freestream velocity, U_∞ [m/s]	30.0
Wing angle of attack, α_w	2° and 10°
Blade pitch at $r/R_p = 0.7$, $\beta_{0.7R_p}$ [°]	30°
Advance ratio, J [-]	0.8
Relative blade-phase angle, $\Delta\phi$ [°]	random, 0, 10, 20, 30, 40 and 50
Rotation direction	co-rotating
Tip clearance d/R_p [-]	≈ 0.05

B. Acoustic measurements

The phased array employed for the experimental campaign consists of 64 *G.R.A.S. 40PH* analog free-field microphones arranged in a configuration described in [27]. The array spans for 1.5 m in the streamwise direction, X, and for 0.4 m along the spanwise direction of the wing, Z, see Fig. 1b. The central microphone of the array is aligned with the location of the wing turning axis at a distance of 0.95 m from its rotational axis, i.e. approximately half the width of the wind-tunnel test section. The furthest downstream and upstream microphones are at an angle of ±40° from the wing turning axis. Along the wing span, the maximum emission angle by the centre propeller covered by microphones is ±22°.

Acoustic data acquisition is controlled with a *National Instruments* (NI) system consisting of four *PXIe-4499* sound and vibration modules with 24-bit resolution and 204.8 kSamples per second maximum sampling rate. These boards are controlled via a NI *PXIe-8370* board. The measurements are acquired at a sampling frequency of 51.2 kHz for a duration of 30 s. Along with the signals of the 64 microphones, pulses of each of the three motor's encoders are also synchronously registered.

III. Methodology

This section provides a thorough overview of the research methodology used in this study, which is aimed at analyzing the impact of synchrophasing on psychoacoustic parameters. The methodology is divided into three main parts: selecting microphones for analysis, processing the acoustic signal using traditional sound metrics, and applying Sound Quality Metrics (SQMs).

A. Selected microphones

From the available array of 64 microphones, microphones A, C, and D (Fig. 4) were specifically chosen for their positions within the array. They were positioned near the $Z/R = 0$ axis, with a side distance of $Y/R = 10.3$. Using $X/R = 0$ as a reference, microphone A was placed upstream with a propagation angle of 52°, microphone C had a propagation angle of 90°, and microphone D was further downstream with the largest propagation angle of 125°. These angles do not account for the convection of the acoustic waves by the freestream, but if the source were in still air, the emission angles for these microphones would be 48°, 85°, and 121°, respectively.

Due to the elliptical layout of the microphone array, these microphones are not perfectly aligned along the same streamwise axis. The vertical distances from the $Z/R = 0$ axis for microphones A and D are $Z/R = 0.098$ and -0.3, respectively. Despite being the furthest from the $Z/R = 0$ axis, microphone D's offset is less than a circumferential directivity angle of 1.3°, making it suitable for this study. By choosing this microphone positioned further downstream, it can capture the acoustic emissions and rotor-rotor interactions after full interaction with the entire setup.

B. Acoustic signal post-processing

The recorded acoustic signals from three different microphones underwent an initial analysis using conventional sound metrics. These signals were first processed using Welch's method to calculate the Power Spectral Density (PSD)

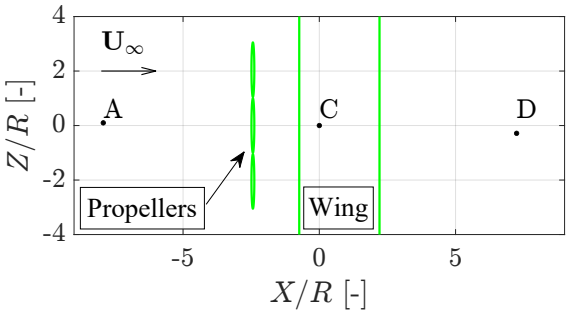

Fig. 4 Microphones A, C and D.

with an 8192 block length, a 50% overlap, and a Hanning window filtering, resulting in frequency spectra with a frequency resolution of $\Delta f = 6.25$ Hz. This information was used to convert the acoustic signals into the sound pressure level (SPL, in dB) using the equation:

$$\mathrm{SPL} = 10 \log_{10} \frac{\mathrm{PSD}(f)\,\Delta f}{p_{\mathrm{ref}}^2} \tag{1}$$

where p_{ref} stands for the reference pressure of 20 μPa. To obtain the Overall Sound Pressure Level (OSPL), the SPL results were integrated with the frequency range of $0.9 \leq \mathrm{BPF} \leq 10$, where BPF refers to the blade-passing frequency. These overall sound pressure levels were converted to A-weighted (OASPL) to reflect human perception of sound better. This process, known as A-weighting, adjusts the sound measurements based on the sound frequency, providing a more accurate representation of the 'loudness' perceived by the human ear.

C. Sound quality metrics

Upon completion of the signal processing using conventional sound metrics, a psychoacoustic analysis was also carried out using sound quality metrics (SQMs). Unlike the sound pressure level (SPL or L_{p}) metric, which quantifies the sound's physical magnitude based on pressure fluctuations, SQMs aim to describe the subjective perception of sound by human hearing. Previous studies [29, 30] showed that these metrics better capture the auditory behavior of the human ear compared to conventional sound metrics typically employed in noise assessments. The five most commonly-used SQMs [31] are:

- Loudness (N): Subjective perception of sound magnitude corresponding to the overall sound intensity [32].
- Tonality (K): Measurement of the perceived strength of unmasked tonal energy within a complex sound [33].
- Sharpness (S): Representation of the high-frequency sound content [34].
- Roughness (R): Hearing sensation caused by sounds with modulation frequencies between 15 Hz and 300 Hz [35].
- Fluctuation strength (FS): Assessment of slow fluctuations in loudness with modulation frequencies up to 20 Hz, with maximum sensitivity for modulation frequencies around 4 Hz [36].

These five SQMs were then combined into a single global psychoacoustic annoyance (PA) metric following the model outlined by Di *et al.* [37].

All the SQMs and the PA metric were computed using the open-source MATLAB toolbox SQAT (Sound Quality Analysis Toolbox) v1.1 [31, 38]. The GitHub repository of the toolbox can be found in [39].

IV. Results

A. Maximum Overall A-weighted Sound Pressure Level ($L_{\mathrm{p,A,max}}$)

Figure 5 shows the impact of the relative blade-phase angle on the maximum OASPL values recorded ($L_{\mathrm{p,A,max}}$). It is evident that the relative blade-phase angle $\Delta\phi$ affects $L_{\mathrm{p,A,max}}$, with a higher reduction in the perceived noise at $\theta = 90°$ and 125°. The maximum $L_{\mathrm{p,A,max}}$ values are observed at $\Delta\phi = 0°$ in all cases, while the minimum levels vary between $\Delta\phi = 20°$ and 30°, depending on the observer position and angle of attack.

For $\alpha_{\mathbf{w}} = 2°$ (Fig. 5a), the difference between the loudest and quietest levels is approximately 4 dBA at $\theta = 52°$. This difference escalates in the downstream direction, to approximately 9 dBA at $\theta = 90°$ and 12 dBA at $\theta = 125°$.

With $\alpha_{\mathbf{w}} = 10°$ (Fig. 5b), the relative blade-phase angle has a considerably smaller impact upstream ($\theta = 52°$), but the $L_{\mathrm{p,A,max}}$ values decrease compared to the noise measured at the same location but at $\alpha_{\mathbf{w}} = 2°$. For $\theta = 90°$ and 125°, the quietest and loudest levels are similar to the $\alpha_{\mathbf{w}} = 2°$ case, with a difference of about 10 dBA. Compared to the random setup, a $\Delta\phi$ equals 0° results in approximately a 3 dBA noise increase for both cases, while the lowest emissions are about 8 dBA quieter.

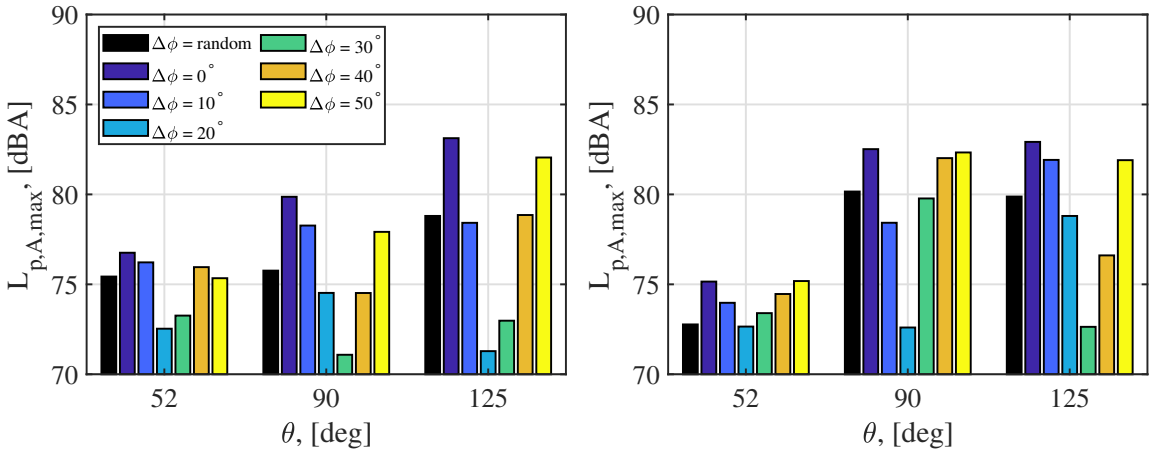

(a) $\alpha_{\mathbf{w}} = 2°$ **(b)** $\alpha_{\mathbf{w}} = 10°$

Fig. 5 Maximum OASPL values as a function of $\Delta\phi$ at $\theta = 52°$, 90° and 125° and for (a) $\alpha_{\mathbf{w}} = 2°$ and (b) 10°.

It is important to highlight that $L_{\mathrm{p,A,max}}$ values for random blade-phase configurations tend to align more with the higher noise levels at $\Delta\phi = 0°$ instead of the lower noise levels near $\Delta\phi = 30°$. Besides, certain blade-phase angles demonstrate consistently lower emissions when compared to the random one for the three directivities tested. The former suggests that synchrophasing could be an effective strategy to reduce perceived noise in distributed-propeller systems if the optimum relative blade-phase angle is chosen.

B. Tone Corrected Perceived Noise Level (PNLT)

The Tone Corrected Perceived Noise Level (PNLT) is an acoustic metric derived from the Perceived Noise Level (PNL). It includes a tone penalty based on the one-third-octave band spectrum, which is an adjustment for sounds with noticeable tonal components [40]. This modification acknowledges that sounds with pronounced tones often seem more irritating or disruptive than the same level of broadband noise.

Figure 6 presents the results using this acoustic metric. For both angles of attack, a small impact on the maximum PNLT values due to changes in the relative blade-phase angle is observed at $\theta = 52°$. However, significant variations in PNLTs are noted at the other two positions. For these angles, trends due to changes in $\Delta\phi$ align with those noted in the $L_{\mathrm{p,A,max}}$ analysis but with smaller differences between the highest and lowest noise levels. However, the PNLT values are higher than those for $L_{\mathrm{p,A,max}}$. This is expected, as this acoustic metric has a tone penalty, and the primary noise in distributed-propeller systems, like the one examined, consists of tonal components.

When comparing the maximum PNLT values at the same propagation angle, there are no significant changes at $\theta = 90°$ and 125° as the angle of attack increases, with a minor increase of about 2 PNLTdB for $\theta = 90°$ values. However, the lowest PNLT values shift from $\Delta\phi = 20°$ to 30° when θ increases to 125°. This pattern is also observed in the $L_{\mathrm{p,A,max}}$ results from Fig. 5.

While both the maximum PNLT and $L_{\mathrm{p,A,max}}$ analyses indicated similar trends associated with changes in the relative blade-phase angle, the PNLT results generally displayed smaller variations between the highest and lowest noise levels.

C. Psychoacoustic Annoyance (PA)

Figure 7 shows the psychoacoustic annoyance values for the cases under investigation. The trends observed here closely replicate the PNLT results. As such, changes in the relative blade-phase angle were negligible for the microphone upstream of the experimental setup ($\theta = 52°$). However, for the other two positions, the relative blade-phase angle had a significant effect.

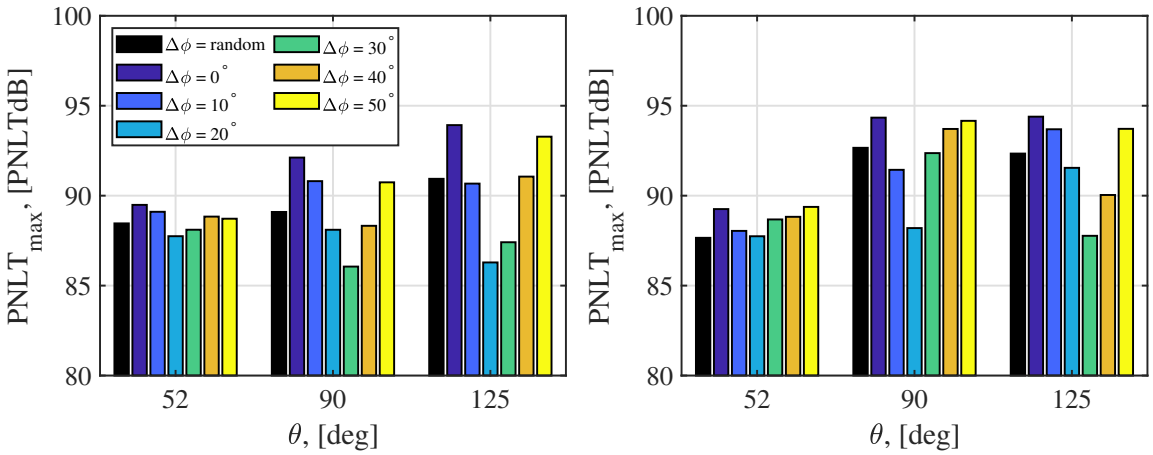

(a) $\alpha_w = 2°$ **(b)** $\alpha_w = 10°$

Fig. 6 Maximum PNLT values as a function of $\Delta\phi$ at $\theta = 52°$, $90°$ and $125°$ and for (a) $\alpha_w = 2°$ and (b) $10°$.

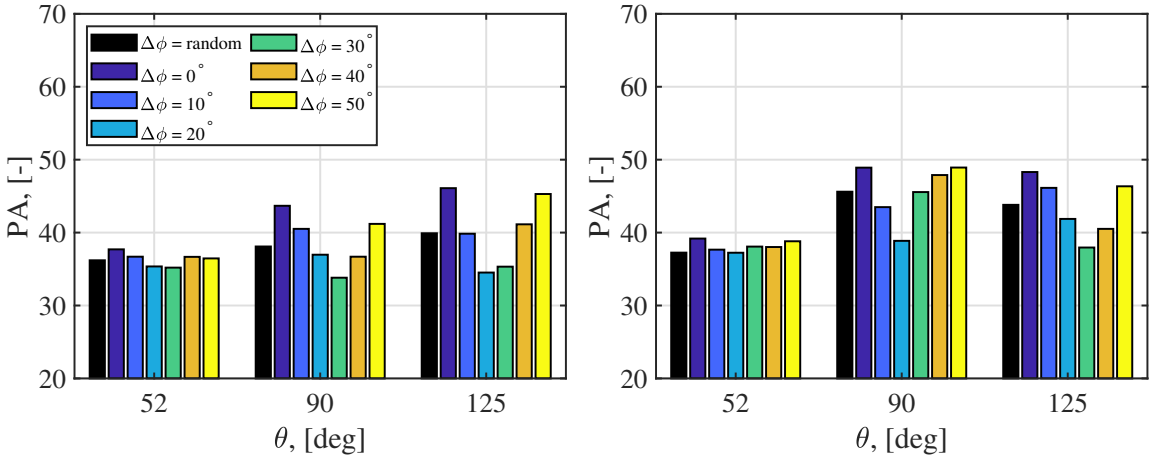

(a) $\alpha_w = 2°$ **(b)** $\alpha_w = 10°$

Fig. 7 5th percentile values of PA as a function of $\Delta\phi$ at $\theta = 52°$, $90°$ and $125°$ and for (a) $\alpha_w = 2°$ and (b) $10°$.

For an angle of attack of 2° (fig. 7a), the highest annoyance level was obtained at a relative blade-phase angle of 0°. This level of annoyance increased as the angle moved in the streamwise direction and was consistently higher than the annoyance levels recorded in random cases. However, different propagation angles did not significantly change the lowest annoyance levels. These values were approximately 34, with less than 3.0% of fluctuation. These lowest levels of annoyance were reached at relative blade-phase angles of either 20° or 30°. This suggests that selecting a relative blade-phase angle between these two values could result in an equivalent level of annoyance at all three positions, which would be close to the minimum possible annoyance level and, therefore, lower than the levels in random cases.

When the angle of attack increased, the minimum annoyance at the three locations rose to about 38, but still with a small fluctuation of less than 2.7%. These minimum annoyance levels were reached again at relative blade-phase angles of either 20° or 30°. This indicates that selecting a relative blade-phase angle between these ranges could yield low annoyance levels, close to the lowest achievable levels, regardless of the angle of attack.

Having gained insights into the psychoacoustic annoyance related to the system, it is important to delve deeper into the impact of the relative blade-phase angle on the individual Sound Quality Metrics (SQMs). The subsequent steps will explore the influence of the relative blade-phase angle on loudness and tonality, as these are considered the most relevant indicators for propeller noise.

D. Loudness (N)

Figure 8 shows how loudness varies with changes in the relative blade-phase angle. While there are differences in levels upstream when the relative blade-phase angle changes, these differences are relatively small. As the polar angle increases, a $\Delta\phi$ equals 20° and 30°, respectively, reduces the levels by about 4 sone compared to the random case. Moreover, a $\Delta\phi$ value of 0° consistently displays the highest loudness, always greater than the random case.

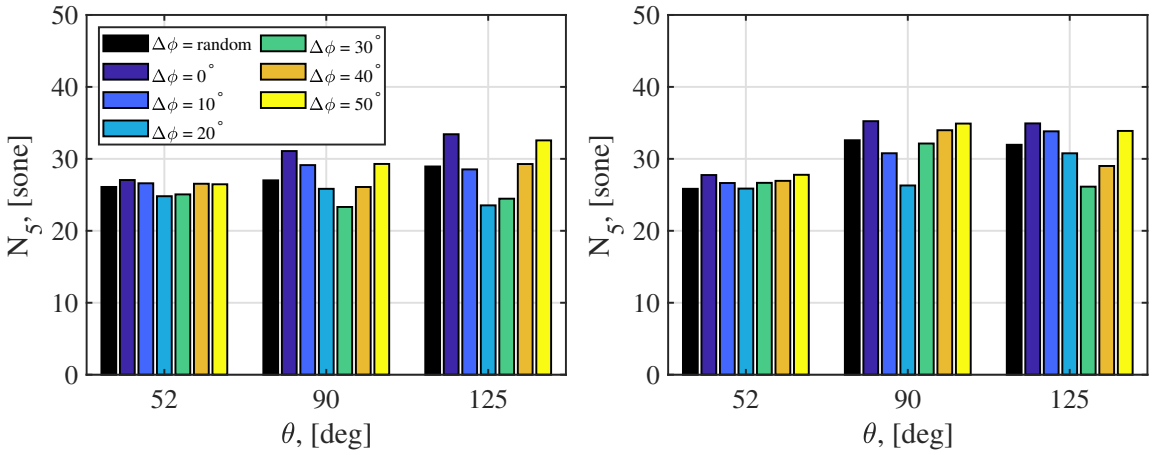

(a) $\alpha_w = 2°$ **(b)** $\alpha_w = 10°$

Fig. 8 5th percentile values of the loudness metric as a function of $\Delta\phi$ at $\theta = 52°$, 90° and 125° and for (a) $\alpha_w = 2°$ and (b) 10°.

E. Tonality (K)

The sound spectrum of this system is primarily characterized by tonal components at the Blade Passing Frequency (BPF), underscoring the relevance of tonality. Moreover, the aerodynamic interference between propellers, related to BPFs, affects the tonal components the system produces. The frequencies of the tones are expected to remain constant between different configurations, but their respective peak levels (and hence tonality) are expected to change with $\Delta\phi$. The broadband surrounding the tones also has an effect on tonality as it can mask the tones and make them less prominent.

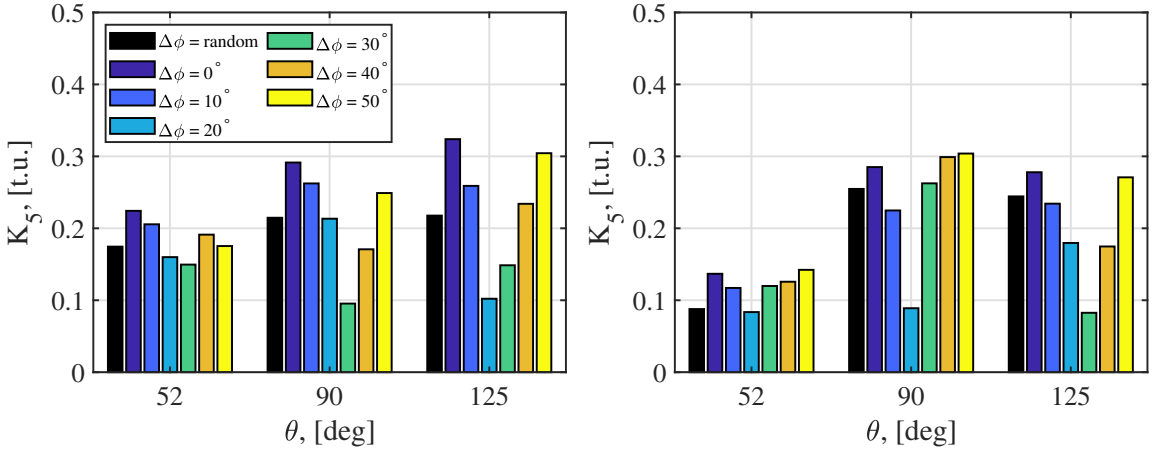

(a) $\alpha_w = 2°$ **(b)** $\alpha_w = 10°$

Fig. 9 5th percentile values of the tonality metric as a function of $\Delta\phi$ at $\theta = 52°$, 90° and 125° and for (a) $\alpha_w = 2°$ and (b) 10°.

Figure 9 shows the effect of changes in the relative blade-phase angle on this factor, presenting noticeable value

fluctuations. Interestingly, the tonality upstream of the model decreases as the angle of attack increases, similar to $L_{p,A,max}$ results. It is worth noting that the highest tonality values are generally recorded for $\Delta\phi = 0°$, except at $\alpha_{\mathbf{w}} = 10°$ and $\theta = 90°$. Under these specific conditions, $\Delta\phi = 40°$ and $50°$ exhibit higher values, but these are still close to the values for $\Delta\phi = 0$. Furthermore, at $\theta = 90°$ and $\theta = 125°$, the lowest tonality levels are half those of the random case levels.

V. Conclusions

This preliminary study explored the effect of the relative blade-phase angle on acoustic metrics, such as the Overall A-weighted Sound Pressure Level ($L_{p,A,max}$), Tone-Corrected Perceived Noise Level (PNLT), Psychoacoustic Annoyance (PA), loudness, and tonality. The relative blade-phase angle significantly influenced these acoustic metrics, with maximum values observed at $\Delta\phi = 0°$. The minimum levels varied between $\Delta\phi = 20°$ and $30°$, suggesting that an optimum relative blade-phase angle between these values could reduce perceived noise in distributed-propeller systems.

Despite similar trends noted in the $L_{p,A,max}$ and PNLT analyses, the latter generally displayed smaller variations between the highest and lowest noise levels. The measurements of the PNLT metric were higher than those in the $L_{p,A,max}$ analysis due to the tone penalty present in the PNLT calculation and the characteristic noise of the system under investigation.

The study of PA suggested that an optimal relative blade-phase angle could be achieved, yielding an equivalent level of annoyance at the three positions investigated, lower than their respective random cases. The results have demonstrated the fundamental importance of considering the adequate sound metric to properly quantify the impact of relative blade-phase angle on the perceived annoyance from the noise generated by the system.

Finally, this research underscores the significance of synchrophasing as an effective strategy to reduce perceived noise generated by a distributed-propulsion system in a tractor configuration. This could be a crucial consideration in designing future aircraft.

Acknowledgments

This work is part of the ENODISE (ENabling Optimized Disruptive Airframe-Propulsion Integration Concepts) project, which has received funding from the European Union's Horizon 2020 research and innovation programme under grant agreement No. 860103. Additionally, this publication is also a part of the *Listen to the future* project (project number 20247), a part of the Veni 2022 research programme (Domain Applied and Engineering Sciences). The latter project is granted to Roberto Merino-Martinez and is (partially) financed by the Dutch Research Council (NWO).

References

[1] "Flightpath 2050 - Europe's Vision for Aviation," Tech. rep., 2011. https://doi.org/10.2777/50266.

[2] Lotinga, M. J., Ramos-Romero, C., Green, N., and Torija, A. J., "Noise from Unconventional Aircraft: A Review of Current Measurement Techniques, Psychoacoustics, Metrics and Regulation," *Current Pollution Reports*, Vol. 9, No. 4, 2023, pp. 724–745. https://doi.org/10.1007/s40726-023-00285-4, URL https://doi.org/10.1007/s40726-023-00285-4.

[3] Rendón, M. A., Sánchez R., C. D., Gallo M., J., and Anzai, A. H., "Aircraft Hybrid-Electric Propulsion: Development Trends, Challenges and Opportunities," *Journal of Control, Automation and Electrical Systems*, 2021. https://doi.org/10.1007/s40313-021-00740-x, URL https://doi.org/10.1007/s40313-021-00740-x.

[4] EASA, "Study on the Societal Acceptance of Urban Air Mobility in Europe," Tech. rep., European Union Aviation Safety Agency (EASA), 2021. URL https://www.easa.europa.eu/full-report-study-societal-acceptance-urban-air-mobility-europe.

[5] Pelz, P. F., Leise, P., and Meck, M., "Sustainable aircraft design - A review on optimization methods for electric propulsion with derived optimal number of propulsors," *Progress in Aerospace Sciences*, , No. xxxx, 2021, p. 100714. https://doi.org/10.1016/j.paerosci.2021.100714.

[6] Stoll, A. M., Bevirt, J. B., Moore, M. D., Fredericks, W. J., and Borer, N. K., "Drag Reduction Through Distributed Electric Propulsion," *14th AIAA Aviation Technology, Integration, and Operations Conference*, Atlanta, GA, 2014, pp. 1–10. https://doi.org/10.2514/6.2014-2851.

[7] Kim, H. D., Perry, A. T., and Ansell, P. J., "A Review of Distributed Electric Propulsion Concepts for Air Vehicle Technology," *2018 AIAA/IEEE Electric Aircraft Technologies Symposium, EATS 2018*, 2018, pp. 1–21. https://doi.org/10.2514/6.2018-4998.

[8] Kim, H. D., Perry, A. T., and Ansell, P. J., "Progress in Distributed Electric Propulsion Vehicles and Technologies," 2020, pp. 1–44.

[9] Borer, N. K., Moore, M. D., and Turnbull, A. R., "Tradespace exploration of distributed propulsors for advanced on-demand mobility concepts," *AIAA AVIATION 2014 -14th AIAA Aviation Technology, Integration, and Operations Conference*, , No. June, 2014, pp. 1–14. https://doi.org/10.2514/6.2014-2850.

[10] Gudmundsson, S., "The Anatomy of the Propeller," *General Aviation Aircraft Design*, Elsevier, 2014, pp. 581–659. https://doi.org/10.1016/b978-0-12-397308-5.00014-3.

[11] Vieira, A., Snellen, M., Malgoezar, A. M. N., Merino-Martinez, R., and Simons, D. G., "Analysis of shielding of propeller noise using beamforming and predictions," *Journal of the Acoustical Society of America*, Vol. 146, No. 2, 2019, pp. 1085–1098. https://doi.org/10.1121/1.5121398, URL https://doi.org/10.1121/1.5121398.

[12] Casalino, D., Diozzi, F., Sannino, R., and Paonessa, A., "Aircraft noise reduction technologies: A bibliographic review," *Aerospace Science and Technology*, Vol. 12, No. 106705, 2008, pp. 1–17. https://doi.org/10.1016/j.ast.2007.10.004, URL https://www.sciencedirect.com/science/article/pii/S1270963807001162.

[13] Magliozzi, B., "Synchrophasing for Cabin Noise Reduction of Propeller-Driven Airplanes," *AlAA 8th Aeroacoustics Conference*, 1983, pp. 1–8. https://doi.org/10.2514/6.1983-717.

[14] Fuller, C. R., "Noise Control Characteristics of Synchrophasing. I - Analytical Investigation," *AIAA Journal*, Vol. 24, No. 7, 1986, pp. 1063–1069. https://doi.org/10.2514/6.1984-2369.

[15] Jones, J. D., and Fuller, C. R., "Noise Control Characteristics of Synchrophasing. II - Experimental Investigation," *AIAA Journal*, Vol. 24, No. 8, 1986, pp. 1271–1276. https://doi.org/10.2514/3.9431.

[16] Pascioni, K. A., Rizzi, S. A., and Schiller, N. H., "Noise Reduction Potential of Phase Control for Distributed Propulsion Vehicles," *AIAA Scitech 2019 Forum*, 2019, pp. 1–16. https://doi.org/10.2514/6.2019-1069.

[17] Patterson, A., Schiller, N. H., Ackerman, K. A., Gahlawat, A., Gregory, I. M., and Hovakimyan, N., "Controller Design for Propeller Phase Synchronization With Aeroacoustic Performance Metrics," *AIAA Scitech 2020 Forum*, 2020. https://doi.org/10.2514/6.2020-1494.

[18] Patterson, A. P., Ackerman, K. A., Hovakimyan, N., and Gregory, I. M., "Trajectory generation for distributed electric propulsion vehicles with propeller synchronization," *AIAA Scitech 2021 Forum*, , No. January, 2021, pp. 1–10. https://doi.org/10.2514/6.2021-0586.

[19] Zhou, W., Ning, Z., Li, H., and Hu, H., "An Experimental Investigation on Rotor-To-Rotor Interactions of Small UAV," *35th AIAA Applied Aerodynamics Conference, 2017*, , No. June, 2017, pp. 1–16. https://doi.org/10.2514/6.2017-3744.

[20] de Vries, R., van Arnhem, N., Sinnige, T., Vos, R., and Veldhuis, L. L., "Aerodynamic Interaction Between Propellers of a Distributed-Propulsion System in Forward Flight," *Aerospace Science and Technology*, Vol. 118, 2021, pp. 1–20. https://doi.org/10.1016/j.ast.2021.107009.

[21] Zarri, A., Koutsoukos, A., and Avallone, F., "Aeroacoustic Interaction Effects of Adjacent Propellers in Forward Flight," *AIAA AVIATION 2023 Forum*, American Institute of Aeronautics and Astronautics, Reston, Virginia, 2023, pp. 1–16. https://doi.org/10.2514/6.2023-4489, URL https://arc.aiaa.org/doi/10.2514/6.2023-4489.

[22] Rizzi, S. A., Huff, D. L., Boyd, D. D. J., Bent, P., B., H., Pascioni, K. A., Sargent, D. C., Josephson, D. L., Marsan, M., He, B., and Snider, R., "Urban Air Mobility Noise: Current Practice, Gaps, and Recommendations," Tech. Rep. NASA Technical Memorandum 83199, NASA, 2020. URL https://ntrs.nasa.gov/api/citations/20205007433/downloads/NASA-TP-2020-5007433.pdf.

[23] Rizzi, S. A., Palumbo, D. L., Rathsam, J., Christian, A., and Rafaelof, M., "Annoyance to noise produced by a distributed electric propulsion high-lift system," *23rd AIAA/CEAS Aeroacoustics Conference, 2017*, , No. June, 2017, pp. 1–17. https://doi.org/10.2514/6.2017-4050.

[24] Serpieri, J., "Cross-Flow Instability: Flow Diagnostics and control of swept wing boundary layers," Ph.D. thesis, Delft University of Technology, 2018. https://doi.org/10.4233/uuid:3dac1e78-fcc3-437f-9579-048b74439f55, URL https://repository.tudelft.nl/islandora/object/uuid:3dac1e78-fcc3-437f-9579-048b74439f55?collection=research.

[25] Remillieux, M. C., Crede, E. D., Camargo, H. E., Burdisso, R. A., J., D. W., Rasnick, M., van Seeters, P., and Chou, A., "Calibration and Demonstration of the New Virginia Tech Anechoic Wind Tunnel," 14^{th} *AIAA/CEAS Aeroacoustics Conference (*29^{th} *AIAA Aeroacoustics Conference), May 5–7, 2008, Vancouver, British Columbia, Canada*, 2008. https://doi.org/10.2514/6.2008-2911, URL http://arc.aiaa.org/doi/pdf/10.2514/6.2008-2911, AIAA paper 2008–2911.

[26] Bento, H. F., Ragni, D., Avallone, F., Simons, D., and Snellen, M., "Acoustic wall treatments for wind tunnel aeroacoustic measurements," *Applied Acoustics*, Vol. 199, 2022, p. 108989. https://doi.org/10.1016/j.apacoust.2022.108989.

[27] Bento, H., Vandercreek, C. P., Avallone, F., Ragni, D., Sijtsma, P., and Snellen, M., "Wall treatments for aeroacoustic measurements in closed wind tunnel test sections," , No. June, 2023, pp. 1–15. https://doi.org/10.2514/6.2023-4162.

[28] Boermans, L. M. M., and Rutten, P. B., "Two-dimensional aerodynamic characteristics of airfoil NLF-MOD22 with fowler flap," Tech. rep., Delft University of Technology, 1995.

[29] Merino-Martinez, R., Pieren, R., and Schäffer, B., "Holistic approach to wind turbine noise: From blade trailing–edge modifications to annoyance estimation," *Renewable and Sustainable Energy Reviews*, Vol. 148, No. 111285, 2021, pp. 1–14. https://doi.org/10.1016/j.rser.2021.111285, URL https://doi.org/10.1016/j.rser.2021.111285.

[30] Merino-Martinez, R., Pieren, R., Schäffer, B., and Simons, D. G., "Psychoacoustic model for predicting wind turbine noise annoyance," 24^{th} *International Congress on Acoustics (ICA), October 24 – 28 2022, Gyeongju, South Korea*, 2022. URL https://www.researchgate.net/publication/364996997_Psychoacoustic_model_for_predicting_wind_turbine_noise_annoyance.

[31] Greco, G. F., Merino-Martinez, R., Osses, A., and Langer, S. C., "SQAT: a MATLAB-based toolbox for quantitative sound quality analysis," 52^{th} *International Congress and Exposition on Noise Control Engineering, August 20 – 23 2023, Chiba, Greater Tokyo, Japan*, International Institute of Noise Control Engineering (I-INCE), ???? URL https://www.researchgate.net/publication/373334884_SQAT_a_MATLAB-based_toolbox_for_quantitative_sound_quality_analysis.

[32] "ISO norm 532–1 – Acoustics – Method for calculating loudness – Zwicker method," Tech. Rep. 1, International Organization for Standardization, 2017. URL https://www.iso.org/obp/ui/#iso:std:iso:532:-1:ed-1:v2:en.

[33] Aures, W., "Procedure for calculating the sensory euphony of arbitrary sound signal. In German: Berechnungsverfahren für den sensorischen Wohlklang beliebiger Schallsignale," *Acustica*, Vol. 59, No. 2, 1985, pp. 130–141. URL https://www.ingentaconnect.com/contentone/dav/aaua/1985/00000059/00000002/art00008.

[34] von Bismark, G., "Sharpness as an attribute of the timbre of steady sounds," *Acta Acustica united with Acustica*, Vol. 30, No. 3, 1974, pp. 159–172. URL https://www.semanticscholar.org/paper/Sharpness-as-an-attribute-of-the-timbre-of-steady-Bismarck/9576a2a74bff46ee0cded25bfd9e4302b4fb0470.

[35] Daniel, P., and Webber, R., "Psychoacoustical Roughness: Implementation of an Optimized Model," *Accustica – acta acustica*, Vol. 83, 1997, pp. 113–123. URL https://www.ingentaconnect.com/contentone/dav/aaua/1997/00000083/00000001/art00020.

[36] Osses, A., García León, R., and Kohlrausch, A., "Modelling the sensation of fluctuation strength," 22^{nd} *International Congress on Acoustics (ICA), September 5 – 9 2016, Buenos Aires, Argentina*, 2016. URL https://pure.tue.nl/ws/portalfiles/portal/52366479/Osses_Garcia_Kohlrausch_ICA2016_ID113.pdf.

[37] Di, G.-Q., Chen, X.-W., Song, K., Zhou, B., and Pei, C.-M., "Improvement of Zwicker's psychoacoustic annoyance model aiming at tonal noises," *Applied Acoustics*, Vol. 105, 2016, pp. 164–170. https://doi.org/10.1016/j.apacoust.2015.12.006, URL http://dx.doi.org/10.1016/j.apacoust.2015.12.006.

[38] Greco, G. F. and Merino-Martinez, R. and Osses, A., "SQAT: a sound quality analysis toolbox for MATLAB (version v1.1)," , May 2024. https://doi.org/10.5281/zenodo.10580337, URL https://zenodo.org/records/10580337, accessed in May 2024.

[39] Greco, G. F. and Merino-Martinez, R. and Osses, A., "SQAT: a sound quality analysis toolbox for MATLAB," , May 2023. URL https://github.com/ggrecow/sqat, accessed in May 2023.

[40] "Federal Aviation Regulations, Part 36 (Appendix 2 to Section A36.4," Tech. rep., Federal Aviation Administration, 800 Independence Avenue, SW, Washington, DC 20591, 2002. URL https://www.faa.gov/documentLibrary/media/Advisory_Circular/AC_36-4D.pdf.